1-1-2014

A computational study of carbon dioxide adsorption on solid boron

Qiao Sun
University of Queensland

Meng Wang
University of Queensland, mw088@uowmail.edu.au

Zhen Li
University of Wollongong, zhenl@uow.edu.au

Aijun Du
Queensland University of Technology

Debra J. Searles
University of Queensland

A computational study of carbon dioxide adsorption on solid boron

Abstract

Capturing and sequestering carbon dioxide (CO_2) can provide a route to partial mitigation of climate change associated with anthropogenic CO_2 emissions. Here we report a comprehensive theoretical study of CO_2 adsorption on two phases of boron, α-B_{12} and γ-B_{28}. The theoretical results demonstrate that the electron deficient boron materials, such as α-B_{12} and γ-B_{28}, can bond strongly with CO_2 due to Lewis acid-base interactions because the electron density is higher on their surfaces. In order to evaluate the capacity of these boron materials for CO_2 capture, we also performed calculations with various degrees of CO_2 coverage. The computational results indicate CO_2 capture on the boron phases is a kinetically and thermodynamically feasible process, and therefore from this perspective these boron materials are predicted to be good candidates for CO_2 capture.

Keywords

dioxide, adsorption, solid, boron, study, computational, carbon

Disciplines

Engineering | Physical Sciences and Mathematics

Publication Details

Sun, Q., Wang, M., Li, Z., Du, A. & Searles, D. J. (2014). A computational study of carbon dioxide adsorption on solid boron. Physical Chemistry Chemical Physics, 16 (25), 12695-12702.

A Computational Study of Carbon Dioxide Adsorption on Solid Boron

Qiao Sun[*,a], Meng Wang[a,b], Zhen Li[*,c], Aijun Du[d] and Debra J. Searles[*,a,e]

Capturing and sequestering carbon dioxide (CO_2) can provide a route to partial mitigation of climate change associated with anthropogenic CO_2 emissions. Here we report a comprehensive theoretical study of CO_2 adsorption on two phases of boron, α-B_{12} and γ-B_{28}. The theoretical results demonstrate that the electron deficient boron materials, such as α-B_{12} and γ-B_{28}, can bond strongly with CO_2 due to Lewis acid-base interactions because the electron density is higher on their surfaces. In order to evaluate the capacity of these boron materials for CO_2 capture, we also performed calculations with various degrees of CO_2 coverage. The computational results indicate CO_2 capture on the boron phases is a kinetically and thermodynamically feasible process, and therefore from this perspective these boron materials are predicted to be good candidates for CO_2 capture.

1 Introduction

Carbon dioxide, CO_2, is a greenhouse gas whose concentration in the atmosphere has been increasing since the industrial revolution, and this increase is largely caused by the burning of fossil fuels. Therefore it is essential that this trend be halted, and new technologies aimed at removing CO_2 from combustion products to reduce its concentration in the atmosphere are being developed.[1,2] An alternative approach to reduction of CO_2 from combustion is to select fuels that produce less CO_2 on combustion than conventional fossil fuels (e.g. natural gas), or no CO_2 (H_2). These fuels often contain contaminants including CO_2, so CO_2 capture from these resources before combustion is necessary and is a well-established process in industry. The most common processes involve treatment with amine solutions or chilled ammonia, however these processes have some problems in that they are not energy efficient, the amine is toxic and solvent can easily be lost.[2,3] In both these approaches to reducing CO_2 in the atmosphere, it is important that new environmentally friendly and economically feasible processes for CO_2 capture be developed.

[a]*Centre for Theoretical and Computational Molecular Science, Australian Institute for Bioengineering and Nanotechnology, The University of Queensland, QLD 4072, Brisbane, Australia. Email: q.sun@uq.edu.au; d.bernhardt@uq.edu.au*

[b]*Center for Bioengineering and Biotechnology, China University of Petroleum (East China), Qingdao 266555, China.*

[c]*Institute of Superconducting & Electronic Materials, The University of Wollongong, NSW 2500, Australia. Email: zhenl@uow.edu.au*

[d]*School of Chemistry, Physics and Mechanical Engineering, Queensland University of Technology, Brisbane, QLD 4001, Australia.*

[e] *School of Chemistry and Molecular Biosciences, The University of Queensland, QLD 4072, Brisbane, Australia.*

Solid adsorbents are anticipated to play a key role in new technologies, and there have been many materials considered in recent years.[4] To be of practical use the materials must be able to strongly adsorb CO_2 and have large surface areas, however many materials only weakly bind CO_2. In this work we find that solid boron materials such as α-B_{12} and γ-B_{28} can adsorb CO_2 strongly and therefore may be useful materials for CO_2 capture.

Boron readily bonds with other boron atoms, forming a variety of different structures with complex features such as three-center two-electron bonds or electron deficient bonds. In the pure boron solids, the B_{12} icosahedron is the basic structural unit which can be flexibly linked or fused to form rigid structures,[5-10] and the existence of this unit and it connectivity is associated with the electron deficiency, or hypovalency, of boron. Four reported boron phases correspond to the pure element: rhombohedral α-B_{12}[6,9,11,12] and β-B_{106}[5] (with 12 and 106 atoms in the unit cell, respectively), tetragonal T-192[7] (with 190–192 atoms per unit cell) and γ-B_{28}[8,13,14] (with 28 atoms in the unit cell), whereas there is a large variety of boron-rich compounds. Much work on boron rich compounds has been carried out due to their physical and chemical properties which have resulted in research for their suitability in applications from nuclear reactors to super-hard, thermoelectric and high-energy materials as well as hydrogen storage materials.[8,12,15-18] In this study, we will investigate CO_2 capture using α-B_{12} and γ-B_{28}. The α-B_{12} phase consists of one B_{12} icosahedron per unit cell and γ-B_{28} consists of icosahedral B_{12} clusters and B_2 pairs in a NaCl-type arrangement.[8] It has been shown that the electronic properties of the B_2 pairs and B_{12} clusters in γ-B_{28}, are different, and this results in charge transfer between them.[8] For α-B_{12} and γ-B_{28}, our study found that there is charge transfer among the atoms on their surfaces and the internal atoms, indicating that the α-B_{12} and γ-B_{28} slabs are amphoteric with acidic and basic sites. The regioselectivity of α-B_{12} and γ-B_{28} indicate CO_2 (Lewis acid) might form strong interactions with the basic sites of their B materials due to Lewis acid-base interactions. In order to test this hypothesis, we have carried out DFT calculations of CO_2 capture on α-B_{12} and γ-B_{28} surfaces. The primary motivation of the theoretical study is to stimulate further experiments to verify our prediction that CO_2 can be captured by these boron materials.

2 Computational methods

Ab initio DFT calculations are performed with the DMol3 module in Material Studio.[19,20] The configurations of CO_2 adsorbed on the boron phases are fully optimized using the generalized gradient approximation[21] treated by the Perdew-Burke-Ernzerhof exchange-correlation potential with long rang dispersion correction carried out using the Grimme's scheme[22]. This method has been used to successfully determine the geometrical, energetic and electronic structural properties of boron clusters, boron phases and boron

containing materials.[23-29] The basis set employed is an all-electron double-numerical atomic orbital basis set, augmented by d-polarization functions (DNP). The cell parameters of α-B_{12} and γ-B_{28} in the calculations are all optimized and are consistent with the experimental values.[8,11] Detailed information on the cell parameters is listed in our previous publication.[27] The slab thicknesses of α-B_{12} and γ-B_{28} are 8.012 Å and 6.914 Å (corresponding to two layers of B_{12} or B_{14} clusters), respectively. The 2 × 2 α-boron (001) and γ-boron (001) surfaces were chosen with a 15 Å vacuum above the slab in order to avoid interactions between their periodic images, and the Brillouin zone is sampled by 6 × 6 × 1 k-points using the Monkhorst-Pack scheme.

The calculations of CO_2 adsorption on α-B_{12} (001) and γ-B_{28} (001) surfaces are based on the fully optimized boron surfaces.[27] The adsorption energy of CO_2 on α-B_{12} and γ-B_{28} are calculated from Eq. 1:

$$E_{ads} = E_{(\text{boron phase}-CO_2)} - E_{CO_2} - E_{(\text{boron phase})} \quad (1)$$

where $E_{(\text{boron phase}-CO_2)}$ is the total energy of the boron surface with a CO_2 molecule adsorbed. In order to better clarify the adsorption and the nature of the interaction of CO_2 with α-B_{12} and γ-B_{28}, atoms in molecules (AIM) theory has been employed in the study. Based on the optimized structures at the DFT-D level, we calculate the wavefunctions at the B3LYP/6-31G(d) level of theory,[21] we then use AIM theory, which has been used to successfully determine intermolecular interactions of different systems.[27,30,31] In the AIM analyses,[32] the existence of an interaction is indicated by the presence of a bond critical point (BCP), and the strength of the bond can be estimated from the magnitude of the electron density (ρ_{bcp}) at the BCP. Similarly, the ring or cage structures are characterized by the existence of a ring critical point (RCP) or cage critical point (CCP). Furthermore, the nature of the molecular interaction can be predicted from the topological parameters at the BCP, such as the the acian of electron density ($\nabla^2\rho_{bcp}$) and energy density (H_{bcp}). The topological analysis of the system was carried out via the AIMALL program.[32]

The transition states between chemisorbed and physisorbed CO_2 have been investigated using the complete LST (linear synchronous transit)/QST (quadratic synchronous transit) method[33] implemented in the DMol3 code. The reactants and products correspond to the optimized structures of CO_2 physisorbed and chemisorbed on α-B_{12} and γ-B_{28} surfaces, respectively. Electron distributions and transfer mechanisms are determined with the Mulliken method.[34]

3 Results and discussion

The α-B_{12} and γ-B_{28} slabs were optimized and the fully relaxed α-B_{12} (001) and γ-B_{28} (001) surfaces with cell vectors are shown in Fig. 1(a) and (b), respectively. We firstly investigated the Mulliken atomic charge distributions on the α-B_{12} (001) and γ-B_{28} (001) surfaces and then carried out a study of the mechanism of CO_2 adsorption on the surfaces of the two boron materials. All the possible sites for CO_2 adsorption on α-B_{12} and γ-B_{28} surfaces have been considered. In this manuscript we will discuss the strongest adsorption sites which we classify as having two different types of interaction: type A and B. In type A interactions, the carbon atom and one oxygen atom in the CO_2 molecule directly connect with two boron atoms, and in type B interactions, two oxygen atoms of the CO_2 molecule directly connect with the boron atoms of the α-B_{12} and γ-B_{28} surfaces.

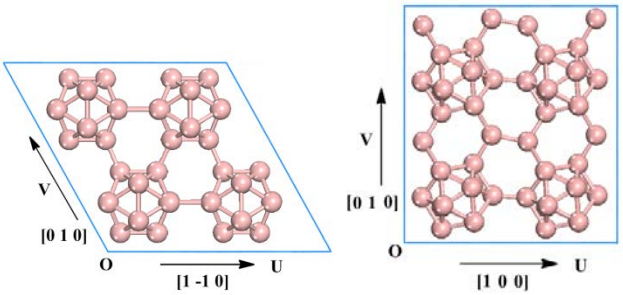

(a) (b)

Fig. 1 The top view of the surfaces of fully relaxed α-B_{12} (001) and γ-B_{28} (001) slabs with cell vectors shown. Atom color code: pink, boron.

3.1 Atomic charge distributions of α-B_{12} and γ-B_{28}

It is well known that boron phases, such as α-B_{12} and γ-B_{28}, are electron deficient materials because there is only one electron on the p orbital of each boron atom, while CO_2 is a Lewis acid and it would prefer to gain electrons in reactions. Because of this the electron deficient boron materials might not be expected to be good adsorbents for CO_2 capture. However, from the Mulliken atomic charge distributions of the α-B_{12} and γ-B_{28} slabs that we modeled we can see that there is electron transfer from the atoms within the slabs to the surface atoms of α-B_{12} and γ-B_{28}. Fig. 2 shows the optimized α-B_{12} and γ-B_{28} structures and the Mulliken atomic charges for the atoms labeled in Fig. 2 are listed in Table 1.

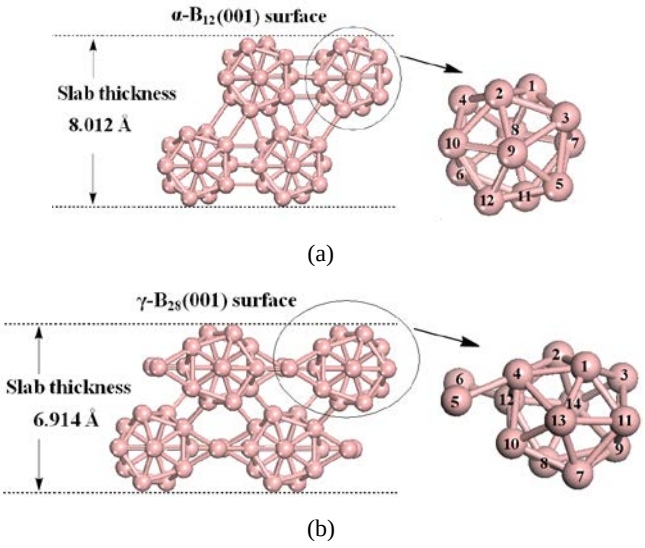

(a)

(b)

Fig. 2 The side view of the optimized α-B_{12} (001) and γ-B_{28} (001) slabs. Mulliken atomic charges of these atoms (with atom numbers in Fig. 2) are listed in Table 1.

The charges on the surface atoms of α-B_{12} are -0.366e (atom B1), -0.321e (atom B2), -0.008e (atom B3 and B4) according to the Mulliken atomic charge analysis, and the atoms in the internal part of the slab have positive charges. The Mulliken atomic charge distributions of γ-B_{28} are similar to those of the α-B_{12} slab: the surface atoms B1 and B2 have negative charges of -0.311e, B3 and B4 have negative charges of -0.098e, and the internal atoms either have positive charges (atoms B9-B14) or are slightly negative

(atoms B7 and B8). The charge difference between the atoms on the surfaces and the internal atoms mean that the α-B_{12} and γ-B_{28} slabs are regioselective and amphoteric, with both acidic and basic sites. Similar behaviour in boron materials, such as B_{80}, has been investigated preciously by Muya et al., who found the cap atoms of B_{80} act as acid sites and the frame atoms act as basic sites in this regioselective molecule.[35] From the above analysis we have shown that, in principle, CO_2 (Lewis acid) will form strong interactions with the basic sites of α-B_{12} and γ-B_{28} due to Lewis acid-base interactions. In the following section, we will investigate CO_2 the mechanism of CO_2 adsorption on the α-B_{12} and γ-B_{28} surfaces.

Table 1 Atom number and Mulliken atomic charges (e) of the optimized α-B_{12} and γ-B_{28} slabs.

α-B_{12}		γ-B_{28}	
Atom number	Atomic charge	Atom number	Atomic charge
B1	-0.366	B1	-0.311
B2	-0.321	B2	-0.311
B3	-0.008	B3	-0.098
B4	-0.008	B4	-0.098
B5	0.139	B5	-0.074
B6	0.139	B6	-0.074
B7	0.119	B7	-0.025
B8	0.119	B8	-0.025
B9	0.033	B9	0.133
B10	0.033	B10	0.133
B11	0.066	B11	0.171
B12	0.055	B12	0.171
		B13	0.204
		B14	0.204

3.2 CO_2 adsorption on the α-B_{12} surface

Currently 16 allotropes of elemental boron have been reported, with the α-boron structure being the simplest.[18] It contains 12 atoms in a rhombohedral unit cell, forming a slightly distorted icosahedral B_{12}. In this section, we will investigate the reaction mechanism of CO_2 adsorption on α-B_{12}. We have identified two ways in which CO_2 adsorbs on α-B_{12}, labelled type A and type B. In type A one O atom and the C atom of CO_2 bond with one B–B bond of α-B_{12}; and in type B two O atoms of CO_2 interact with one B–B bond of α-B_{12}.
Fig. 3 (a) shows the optimized structures of the two possible minimum-energy type A configurations, and the transition states for the process of CO_2 adsorption on the α-B_{12} surface. Corresponding results for type B interactions have been listed in the supporting information, see Fig. S1 (a). The important structural properties, relative energies and the electron transfers from the α-B_{12} to CO_2 are listed in Table 2 and Table S1 in supporting information. For the two types of interaction of CO_2 with α-B_{12}, we can see that the chemisorbed type A configuration is the most stable, so the discussion will focus on the adsorption through interactions of type A. For CO_2 capture on α-B_{12} through type A interactions, we identified two stationary states, corresponding to physisorption and chemisorption. In the physisorbed configuration, CO_2 interacts with one B–B bond of α- B_{12} and lies parallel to it. The O–C–O angle is 179.9° and B–O distance is approximately 3.1 Å, the long distance indicates the interaction is very weak and the adsorption is mainly due to the van der Waals interaction of CO_2 and α-B_{12}.

Table 2 Adsorption energy in kcal/mol, bond distance (r) in Å, bond angle (α) in deg and charge transfer (CT) in electrons for the type A of CO_2 adsorption on α-B_{12} and γ-B_{28} surfaces.

Chem		Phys	TS	Chem
α-B_{12} surface	Adsorption energy	-4.95	-0.46	-47.76
	r(B–O1)	3.042	1.967	1.477
	r(B–C)	3.107	2.648	1.647
	r(C–O1)	1.176	1.208	1.442
	r(C–O2)	1.176	1.170	1.203
	r(B–B)	1.597	1.636	1.694
	α(O–C–O)	179.9	170.5	122.7
	CT	0.004	0.05	-0.584
γ-B_{28} Surface	Adsorption energy	-4.84	-2.50	-29.18
	r(B–O1)	2.896	1.738	1.482
	r(B–C)	3.304	2.616	1.649
	r(C–O1)	1.178	1.216	1.413
	r(C–O2)	1.175	1.166	1.206
	r(B–B)	1.671	1.672	1.740
	α(O–C–O)	179.7	168.8	123.4
	CT	0.007	0.077	-0.528

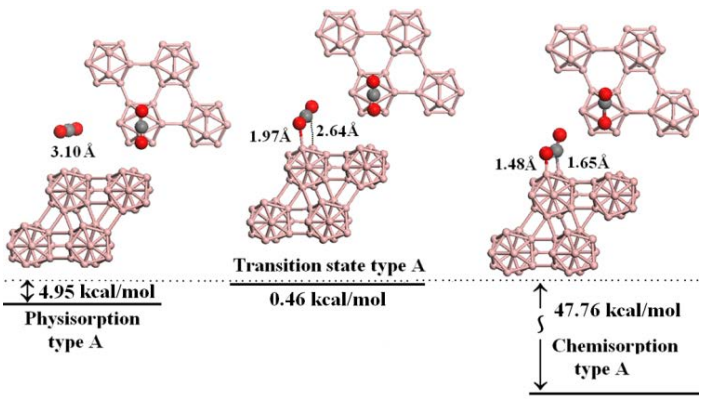

(a)

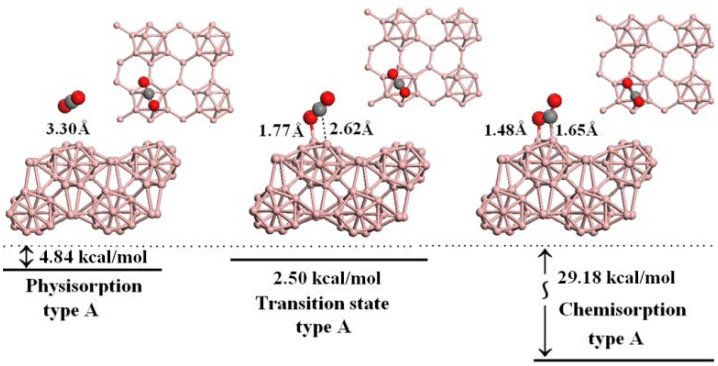

(b)

Fig. 3 Computed minimum energy configurations and transition state for CO_2 adsorption on the α-B_{12} (a) and γ-B_{28} (b) surfaces involving type A interactions (top and side view of the two minimum energy configurations and transition state).

Table 3 Atom number and Mulliken atomic charges (e) and the sum of charge (e) of CO_2, the boron cell of α-B_{12}_CO_2 and γ-B_{28}_CO_2 complexes (chemisorbed configurations) as well as the charge transfer of α-B_{12}_CO_2 (CT1) and γ-B_{28}_CO_2 (CT2) complexes comparing with those of the isolated forms.

Atom type/Sum	CO_2	α-B_{12}	CT1	γ-B_{28}	CT2

of charge		_CO_2		_CO_2	
O1	-0.284	-0.481	-0.197	-0.460	-0.263
C	0.568	0.246	-0.322	0.278	0.600
O2	-0.284	-0.349	-0.065	-0.346	-0.281
Sum of charge	0.0	-0.584		-0.528	
B1		-0.186	0.180	-0.192	0.119
B2		0.110	0.431	0.065	0.376
B3		0.001	0.009	-0.011	0.087
B4		0.000	0.008	-0.007	0.091
B5		0.036	-0.103	-0.098	-0.024
B6		0.036	-0.103	-0.057	0.017
B7		0.071	-0.048	-0.010	0.015
B8		0.071	-0.048	-0.018	0.007
B9		0.082	0.049	0.125	-0.008
B10		0.081	0.048	0.126	-0.007
B11		0.069	0.003	0.095	-0.076
B12		0.057	0.002	0.116	-0.055
B13				0.093	-0.111
B14				0.077	-0.127
Sum of charge		0.428		0.304	

The adsorption energy of the physisorbed CO_2 is calculated to be 4.95 kcal/mol. The weak interaction is also confirmed by the negligible charge transfer between the α-B_{12} and CO_2 molecule (with a value of only -0.004e). Molecular graphs for CO_2 adsorption on α-B_{12} are displayed in Fig. 4. We can see from Fig. 4 (a) that the interaction between CO_2 and α-B_{12} can be confirmed by the existence of the bond critical point (BCP) of the O–B contact. The calculated topological parameters at the BCPs of the α-B_{12} are listed in Table S2 in supporting information. For the physisorbed configurations, the electron densities at the BCPs of the bonds between CO_2 and α-B_{12} are small (Table S2), which is consistent with a weak interaction. When CO_2 is chemisorbed on α-B_{12}, the B–C and B–O bond lengths shorten and a four-membered ring is formed. The O–C–O bond angle is 122.7°, and one C=O double-bond breaks and stretches from 1.176 Å to 1.442 Å due to the bonding interaction that is formed between the B–B bond of α-B_{12} and C–O bond of CO_2. Table 3 lists the Mulliken atomic charges (e) of the α-B_{12}–CO_2 and γ-B_{28}–CO_2 complexes (chemisorbed configurations) and the charge transfers of CO_2 and the boron cells which directly connect with CO_2 of α-B_{12}–CO_2 (CT1) and γ-B_{28}–CO_2 (CT2) complexes comparing with those of the isolated forms. A Mulliken charge population analysis shows that there is -0.584 electron charge transfer from α-B_{12} to the CO_2 molecule, and the charge redistributions of the boron atoms at the CO_2/B interface is the main contribution for the charge transfer. The CO_2 molecule undergoes structural distortion to a bent geometry and forms a C–O–B–B four-membered ring, in which the B–C and B–O distances are 1.647 Å and 1.477 Å, respectively. The short distance indicates a strong interaction between the CO_2 molecule and α-B_{12}, with the calculated adsorption binding energy is 47.76 kcal/mol.

Here we note that the interaction between CO_2 and α-B_{12} is the strongest value for CO_2 adsorption on substrates so far, as far as we are aware. Moreover, the calculated barrier between the physisorbed and chemisorbed configurations is 4.49 kcal/mol. As shown in Table S2, as we move from the physisorbed configuration (Fig. 4(a)), to the transition state (Fig. 4(b)), to the chemisorbed configuration (Fig. 4(c)) the electron densities at the BCPs for the O1–B bonds increase, which is consistent with the adsorption process resulting in strengthening of the interaction. In addition, the O1–B bond distances decrease from 3.042 Å for the physisorbed structure, 1.967 Å for the transition state structure and 1.477 Å when the CO_2 is chemisorbed, and the C–B bond distances decrease with the values of 3.107 Å, 2.648 Å and 1.647 Å for the three structures, respectively. The strong interaction between CO_2 and α-B_{12}, and low barrier from the physisorbed to chemisorbed configurations demonstrate that the CO_2 adsorption on α-B_{12} is a kinetically favorable process. In addition, we have listed variation of thermodynamic properties with temperatures (K) for adsorption of free CO_2 on the α-B_{12} (a) and γ-B_{28} (b) surfaces to form chemisorbed configurations (type A) in Figure 5. Fig. 5 (a) shows the temperature dependence of thermodynamic properties ΔG (kcal/mol), ΔH (kcal/mol) and ΔS (cal/mol K) for gaseous CO_2 capture on α-B_{12} to form a chemisorbed configuration of type A. It clearly shows that the ΔS of the reaction increases as temperature increases from 200 to 1000 K and ΔH is almost constant over the whole temperature range. The resulting negative ΔG indicates the adsorption reaction process is spontaneous for the temperatures considered.

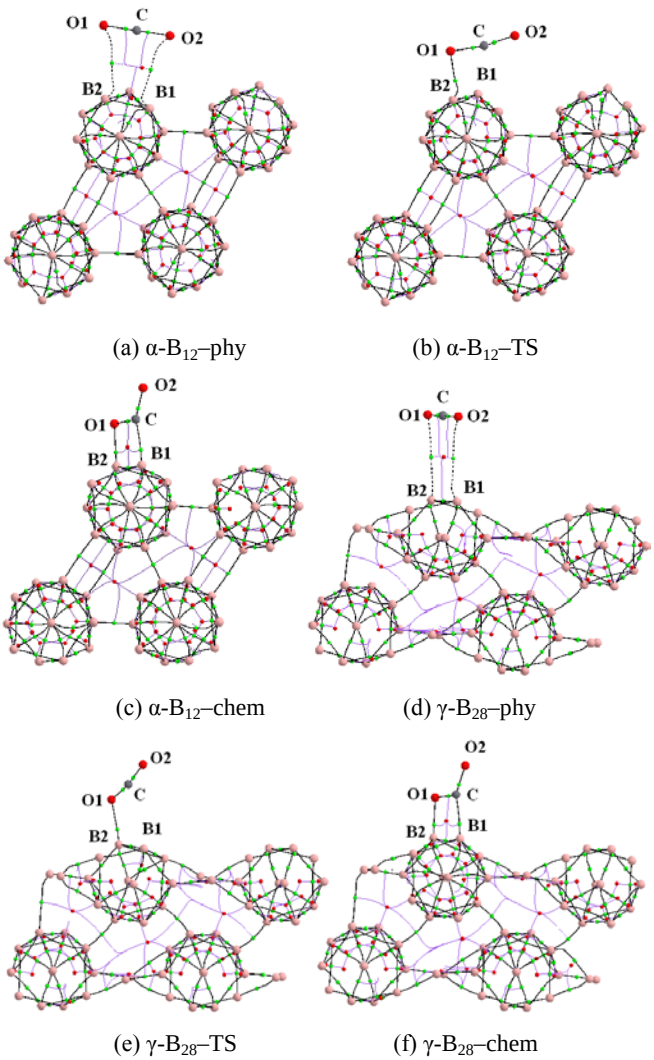

(a) α-B_{12}–phy (b) α-B_{12}–TS

(c) α-B_{12}–chem (d) γ-B_{28}–phy

(e) γ-B_{28}–TS (f) γ-B_{28}–chem

Fig. 4 The molecular graphs of the minimum energy structures and transition states of CO_2 adsorbed on the α-B_{12} and γ-B_{28} surfaces with type A interactions, where the bond critical points (BCPs), ring critical points (RCPs) and cage critical point (CCP) are denoted as small green, red and blue dots, respectively.

For type B interactions of CO_2 with α-B_{12}, we also identified two local minima and the transition state between those physisorbed and chemisorbed states. The physisorbed configuration (Fig. S1(a)) of CO_2 on α-B_{12} is very similar to that observed in the type A physisorbed configuration. The chemisorbed configuration (Fig. S1(a)) has a O–C–O–B–B five-membered ring. In this configuration, the two C–O bonds have stretched from 1.176 Å to 1.330 Å and the

O–C–O bond angle is 115.4°. The B–B site is also pulled out of the material and elongated by 0.10 Å. The two B–O distances are 1.494 Å which is slight longer than the O–B distance in the type A configuration for α-B_{12} (1.447 Å). The adsorption energy of this chemisorbed configuration is 41.81 kcal/mol, which is slightly weaker than that for type A. The calculated barrier between the physisorbed and chemisorbed configurations is 6.16 kcal/mol. The strong interaction and low barrier between the physisorbed and chemisorbed configurations with type B interactions indicates CO_2 capture is feasible through this mechanism. However, the CO_2 capture process involving type A interactions will dominate because it has a stronger interaction energy and lower barrier to adsorption than type B interactions. Overall, the calculations demonstrate that the α-B_{12} phase can effectively capture CO_2.

3.3 CO_2 adsorption on γ-B_{28} surface

The γ-B_{28} phase with 28 atoms in the orthorhombic unit cell was originally discovered in 1965,[14] and is a hard semiconductor with a structure composed of B_2 dumbbells and B_{12} icosahedra. There is debate about whether the two distinct structural units should be partially ionic or not.[13,24,36] Our Mulliken charge analysis of the γ-B_{28} (001) slab indicate that the γ-B_{28} is amphoteric which contains both acidic and basic sites. This means that the electron deficient boron phase γ-B_{28} could denote electrons from its basic sites to CO_2 to form a strong bond between CO_2 and the basic sites of γ-B_{28}, and therefore γ-B_{28} might be a good candidate for CO_2 capture. In this section, we will discuss the absorption of CO_2 on the γ-B_{28} surface. The computational results indicate that there are two types (A and B) of adsorption of CO_2 on γ-B_{28} surface, which are very similar to those seen in CO_2 adsorption on α-B_{12}. Firstly, we will discuss CO_2 adsorption on γ-B_{28} involving type A interactions. We identified two stationary states corresponding to physisorbed and chemisorbed CO_2. The optimized structures of the two configurations as well as the transition state between them are shown in Fig. 3(b). The important structural properties, adsorption energies and the electron transfers from the boron phase to CO_2 are listed in Table 2. From Fig. 3(b) we can see that the CO_2 physisorbs by interaction with one B–B bond of γ-B_{28}, and is parallel to that bond. The O–C–O angle is 179.7° and the B–O distance is around 2.9 Å. The structure is very similar to that of the configuration of CO_2 physisorbed on α-B_{12} in a type A interaction (Fig. 3(a)). The adsorption energy of the physisorbed CO_2 is calculated to be 4.84 kcal/mol so the interaction between CO_2 and γ-B_{28} is very weak.

In its chemisorbed configuration, the CO_2 molecule undergoes structural distortion to a bent geometry and forms a C–O–B–B four-membered ring in which the B–C and B–O distances are 1.649 Å and 1.482 Å, respectively. The O–C–O bond angle is 123.4°, and one C=O double-bond breaks and stretches from 1.178 Å to 1.413 Å due to the bonding interaction that formed between the B–B bond of the γ-B_{28} and the C–O bond of CO_2. The shorter distance indicates a stronger interaction between the CO_2 molecule and γ-B_{28}, and the calculated adsorption energy is 29.18 kcal/mol. Compared with the type A energy of adsorption of CO_2 on α-B_{12} (47.76 kcal/mol), the adsorption of CO_2 on γ-B_{28} is much lower. The transition state between the physisorbed and chemisorbed configurations has been identified. Adsorption has also been verified by observation of an increase in the energy density at the BCP in going from the physisorbed state (Fig. 4(d)), to the transition state (Fig. 4(e)), and to chemisorbed state (Fig. 4(f)), which is consistent with strengthening of the interaction. In addition, the O1–B bond distances decrease from 2.896 Å to 1.738 Å and then 1.482 Å, and the C–B bond distances decrease from 3.304 Å to 2.616 Å and then 1.649 Å for the three structures, respectively. The calculated barrier between the physisorbed and chemisorbed configurations with type A interactions is 2.34 kcal/mol. The variation of thermodynamic properties has also been calculated (Fig. 5(b)) in order to study the entropic and temperature effects of the chemisorption of gaseous CO_2 on γ-B_{28}. From Fig. 5(b) we can see that ΔS is monotonically increasing when the temperature is above 200 K and ΔH has a slight linear increase over the whole temperature range considered. This results in ΔG increasing almost linearly with an increase in temperature for CO_2 capture on γ-B_{28}, as the free CO_2 is chemisorbed on the surface. Moreover, ΔG is negative in the temperature range considered (200 K to 1000 K), which indicates the adsorption of CO_2 on γ-B_{28} to form the chemisorbed configuration is a spontaneous process for these temperatures. In summary, the low barrier and the negative ΔG within the temperature range demonstrate that CO_2 adsorption on γ-B_{28} is a kinetically and thermodynamically favorable process.

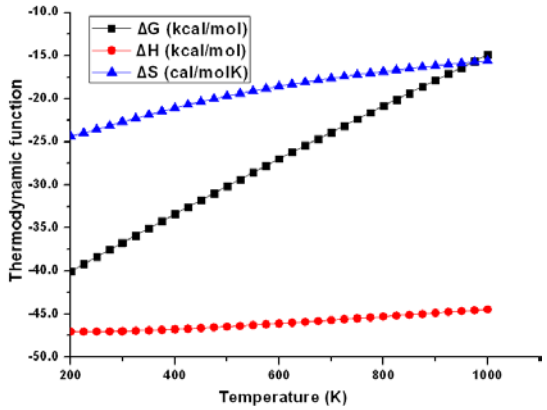

(a)

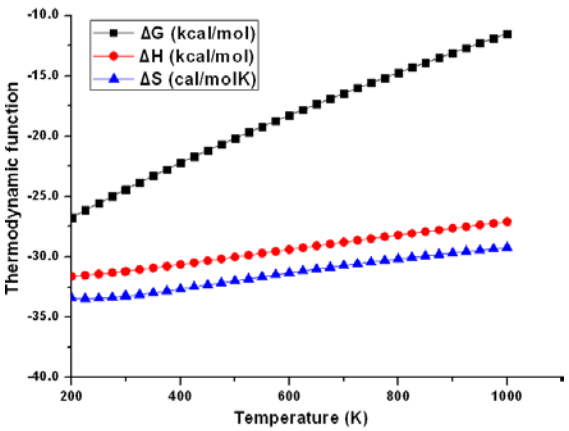

(b)

Fig. 5 Variation of thermodynamic properties with temperatures (K) for adsorption of free CO_2 on the α-B_{12} (a) and γ-B_{28} (b) surfaces to form chemisorbed configurations (type A). Squares, triangles and circles correspond to the change in Gibbs free energy (kcal/mol), change in entropy (cal/mol K) and change in enthalpy (kcal/mol), respectively.

For CO_2 capture on γ-B_{28} with type B interactions, two local minima were also observed (chemisorbed and physisorbed configurations). In the physisorbed configuration, CO_2 weakly interacts with γ-B_{28} with the adsorption energy of 4.89 kcal/mol. The chemisorbed CO_2 on γ-B_{28}, has one five-membered ring O–C–O–B–B, which is very similar to that of configuration of chemisorbed on CO_2 on α-B_{12} with type B interactions. In this configuration, the two C–O bonds stretch from 1.176 Å to 1.314 Å and the O–C–O bond angle is 117.6°. The

B–B site is also pulled out and elongated by 0.10 Å. The two B–O distances are 1.511 Å, which is slight longer than that of O–B distance when type A interactions result in CO_2 bonding to γ-B_{28} (1.482 Å). The adsorption energy of this chemisorbed configuration is 21.78 kcal/mol, which is slightly weaker than the absorption energy of the type A chemisorbed configuration. The barrier from the physisorbed to chemisorbed configurations with the type B configuration is low with a value of 9.39 kcal/mol. Moreover, the type A configuration will be the dominant one because it has a stronger adsorption energy and lower barrier than that due to type B interactions. In all, the computational results support the hypothesis that the γ-B_{28} phase can effectively capture CO_2.

The different adsorption energies between CO_2 and the two boron phases can be understood by analysis of their LUMO-HOMO energy gaps. According to molecular orbital theory, the frontier orbits and nearby molecular orbits are the most important factors determining the stability of molecules. The larger the difference between the frontier orbits, the more stable the molecular structure is. The energy gaps of ΔE between their highest occupied molecular orbitals (HOMO) and their lowest unoccupied molecular orbitals (LUMO) ($\Delta E = E_{LUMO} - E_{HOMO}$) for α-$B_{12}$ and γ-B_{28} surfaces are 0.046 and 0.854 eV, respectively. The energy gap of γ-B_{28} is clearly larger than that of α-B_{12}. The narrower LUMO-HOMO energy-gap indicates that this material is more reactive. The interaction of CO_2 with α-B_{12} (adsorption energy 47.76 kcal/mol for the type A configuration) is stronger that with γ-B_{28} (adsorption energy 29.18 kcal/mol for the type A configuration). The energy gaps of the two boron materials explains the relative strength of interactions between them and CO_2. Moreover, from the Mulliken charge analysis we know that the charges of the surface atoms B1 and B2 of α-B_{12} which interact directly with CO_2 are -0.366e and -0.321e, while the charges of two boron atoms of γ-B_{28} which interact directly with CO_2 with are -0.311e and -0.311e, respectively, which also indicate the base sites of the α-B_{12} surface are more basic than those of γ-B_{28} surface. The charge analysis is also consistent with the Lewis acid-base interaction of CO_2 on the α-B_{12} surface being stronger than that of CO_2 with the γ-B_{28} material.

3.4 Coverage of CO_2 on α-B_{12} and γ-B_{28} surfaces

In the previous calculations, adsorption of one CO_2 molecule on the 2 × 2 α-B_{12} and γ-B_{28} surfaces was considered. In order to investigate the capacity of these boron materials for CO_2 capture, calculations with higher coverage of CO_2 have been carried out.

The average adsorption energies of CO_2 molecules on boron surfaces are defined as

$$E_{ads} = (E_{(\text{boron phase–n}CO_2)} - nE_{CO_2} - E_{(\text{boron phase})})/n \quad (2)$$

where n is the number of CO_2 molecules adsorbed on the boron surfaces and $E_{(\text{boron phase–n}CO_2)}$ is the total energy of the boron surface with CO_2 adsorbed.

Table 4 and Figure 6 list the structural properties and the absolute value of average adsorption energies (kcal/mol) with different coverage of CO_2 on α-B_{12} and γ-B_{28} surfaces with up to four molecules of CO_2. We find that the α-B_{12} and γ-B_{28} surfaces can effectively capture up to four CO_2 molecules through chemisorption with configurations which are similar to those when one CO_2 is

Table 4 The absolute value of average adsorption energies in kcal/mol, average bond distances (r) in Å, bond angles (α) in deg and charge transfer (CT) in electron for two, three and four CO_2 molecules adsorption on α-B_{12} and γ-B_{28} surfaces.

Adsorbents	Properties	Two CO_2	Three CO_2	Four CO_2
α-B_{12} surface	Ads	-43.19	-38.09	-33.79
	r(B–O1)	1.473	1.479	1.481
	r(B–C)	1.650	1.661	1.675
	r(C–O1)	1.430	1.407	1.388
	r(C–O2)	1.201	1.202	1.201
	r(B–B)	1.700	1.703	1.711
	α(O–C–O)	123.4	124.6	125.9
	CT	-0.514	-0.444	-0.388
γ-B_{28} Surface	Ads	-27.61	-25.25	-24.29
	r(B–O1)	1.462	1.470	1.471
	r(B–C)	1.642	1.662	1.666
	r(C–O1)	1.435	1.408	1.198
	r(C–O2)	1.200	1.200	1.406
	r(B–B)	1.740	1.743	1.744
	α(O–C–O)	123.1	124.6	125.1
	CT	-0.489	-0.442	-0.408

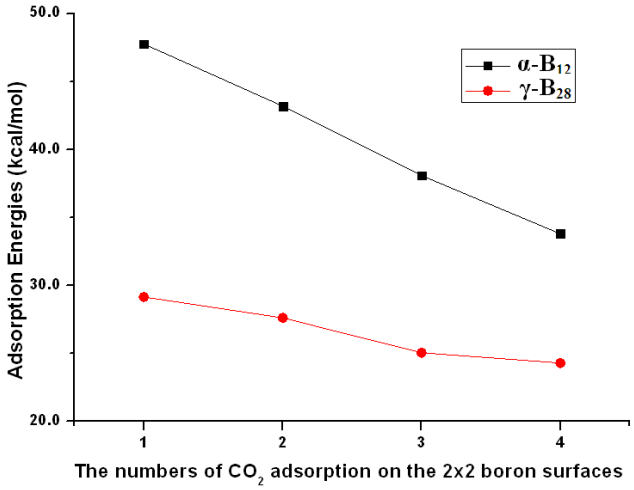

Fig. 6 The absolute value of average adsorption energies (kcal/mol) with two, three and four CO_2 molecules adsorption on 2 × 2 α-B_{12} and γ-B_{28} surfaces.

adsorbed on these surfaces. However, the average adsorption energies reduce with increasing of CO_2 coverage. In detail, the adsorption energies for CO_2 molecules adsorbed on 2 × 2 α-B_{12} reduce from -47.76 to -33.79 kcal/mol as the number of CO_2 molecules increases from one to four, with the energy required to remove one CO_2 molecule from the system with four adsorbed being -20.89 kcal/mol. As the number of CO_2 molecules adsorbed on 2 × 2 γ-B_{28} increases from one to four, the average adsorption energies reduce from -29.19 to -24.29 kcal/mol, with the energy required to remove one CO_2 molecule from the system with four adsorbed being -21.41 kcal/mol. These results indicate that the binding of additional CO_2 molecules will be weaker. This means that although the energy required to completely regenerate the clean boron would be high, boron solid which is partly covered by CO_2 molecules would be a useful material for CO_2 capture. Therefore pure solid boron could be used a material for permanent capture of CO_2; or alternatively the solid boron functionalised with CO_2 could be used as a material for capture of further CO_2 and release of the additional CO_2.

4 Conclusions

Using DFT calculations we have investigated the reaction mechanisms for CO_2 capture on α-B_{12} and γ-B_{28} surfaces. We found that these "electron deficient" boron solids perform well in capturing CO_2 on the basic sites of these boron surfaces due to Lewis acid-base interactions. The absorption energy of CO_2 with their strongest adsorption configurations on α-B_{12} and γ-B_{28} boron phases are 47.76 and 29.18 kcal/mol, respectively, and the barriers of these adsorption processes from their physisorbed to chemisorbed configurations are very low. Moreover, the values of the changes of Gibbs free energy for capture of free CO_2 on α-B_{12} and γ-B_{28} surfaces to form chemisorbed configurations are negative over the temperature range 200 ~ 1000 K, which indicate the reactions are spontaneous within this temperature range. The calculations also show the binding between CO_2 and the materials become weaker as the CO_2 coverage increases. In addition, the modelling suggests that the solid boron materials can effectively capture CO_2, and should stimulate some further experiments to verify our theoretical prediction.

Acknowledgements

Q. S. and M. W acknowledge financial support from Early Career Researcher grant of The University of Queensland. A. D. greatly appreciates financial support of the Australian Research Council QEII Fellowship. We also acknowledge generous grants of high performance computer time from both The University of Queensland and the National Computational Infrastructure (NCI).

Notes and references

1. D. W. Keith, *Science* 2009, ***325***, 1654.
2. R. S. Haszeldine, *Science* 2009, ***325***, 1647.
3. R. J. Hook, *Ind. Eng. Chem. Re.* 1997, ***36***, 1779.
4. Y. Belmabkhout and A. Sayari, *Chem. Eng. Sci.* 2009, ***64***, 3729.
5. D. E. Sands and J. L. Hoard, *J. Am. Chem. Soc.* 1957, ***79***, 5582.
6. L. V. McCarty, J. S. Kasper, F. H. Horn, B. F. Decker and A. E. Newkirk, *J. Am. Chem. Soc.* 1958, ***80***, 2592.
7. C. P. Talley, *Acta Cryst.* 1960, ***13***, 271.
8. A. R. Oganov, J. Chen, C. Gatti, Y. Ma, Y. Ma, C. W. Glass, Z. Liu, T. Yu, O. O. Kurakevych and V. L. Solozhenko, *Nature* 2009, ***457***, 863.
9. D. Li, Y. N. Xu and W. Y. Ching, *Phys. Rev. B* 1992, ***45***, 5895.
10. J. L. He, E. D. Wu, H. T. Wang, R. P. Liu and Y. J. Tian, *Phys. Rev. Lett.* 2005, ***94***, 015504.
11. G. Will and B. Kiefer, *Z. Anorg. Allg. Chem.* 2001, ***627***, 2100.
12. A. R. Oganov and V. L. Solozhenko, *J. Superhard Mat.* 2009, ***31***, 285.
13. U. Häussermann and A. S. Mikhaylushkin, *Inorg. Chem.* 2010, ***49***, 11270.
14. R. H. Wentorf, *Science* 1965, ***147***, 49.
15. Y. Wang and G. H. Robinson, *Science* 2011, ***333***, 530.
16. B. Marlid, K. Larsson and J. O. Carlsson, *J. Phys. Chem. B* 2001, ***105***, 12797.
17. M. Li, Y. Li, Z. Zhou, P. Shen and Z. Chen, *Nano Lett.* 2009, ***9***, 1944.
18. P. Wagner, C. P. Ewels, I. Suarez-Martinez, V. Guiot, S. F. J. Cox, J. S. Lord and P. R. Briddon, *Phys. Rev. B* 2011, ***83***, 024101.
19. B. Delley, *J. Chem. Phys.* 1990, ***92***, 508.
20. B. Delley, *J. Chem. Phys.* 2000, ***113***, 7756.
21. J. P. Perdew, K. Burke and M. Ernzerhof, *Phys. Rev. Lett.* 1996, ***77***, 3865.
22. S. Grimme, *J. Comput. Chem.* 2006, ***27***, 1787.
23. N. G. Szwacki, A. Sadrzadeh and B. I. Yakobson, *Phys. Rev. Lett.* 2007, ***98***, 166804.
24. D. Prasad and E. D. Jemmis, *Phys. Rev. Lett.* 2008, ***100***, 165504.
25. A. K. Singh, A. Sadrzadeh and B. I. Yakobson, *Nano Lett.*, 2008, ***8***, 1314.
26. Q. Sun, Z. Li, D. J. Searles, Y. Chen, G. Q. Lu and A. J. Du, *J. Am. Chem. Soc.* 2013, ***135***, 8246.
27. Q. Sun, M. Wang, Z. Li, P. Li, W. H. Wang, X. J. Tan and A. J. Du, *Fuel* 2013, ***109***, 575.
28. Q. Sun, M. Wang, Z. Li, Y. Y. Ma and A. J. Du, *Chem. Phys. Lett.* 2013, ***135***, 59.
29. Q. Sun, M. Wang, Z. Li, A. J. Du, D. J. Searles, *J. Chem. Phys. C*, 2014, ***118***, 2170.
30. Q. Sun, Z. Li, M. Wang, A. Du and S. C. Smith, *Chem. Phys. Lett.* 2012, ***550***, 41.
31. Q. Sun, Z. Li, A. Du, J. Chen, Z. Zhu and S. C. Smith, *Fuel* 2012, ***96***, 291.
32. R. F. W. Bader, *Atoms in Molecules: A Quantum Theory*, Oxford University Press, Oxford, **1990**.
33. T. A. Halgren and W. N. Lipscomb, *Chem. Phys. Lett.* 1977, ***49***, 225.
34. R. S. Mulliken, *J. Chem. Phys.* 1955, ***23***, 1833.
35. J. T. Muya, F. De Proft, P. Geerlings, N. Minh Tho and A. Ceulemans, *J. Phys. Chem. A* 2011, ***115***, 9069.
36. J. S. Tse, *Nature* 2009, ***457***, 800.